Arctic Ocean tides from GRACE satellite accelerations

E.Killett, [1,2] J. Wahr,[1] S. Desai,[2] D. Yuan,[2] and M. Watkins[2]

Received 11 March 2011; revised 17 August 2011; accepted 19 August 2011; published 4 November 2011.

[1] Models are routinely used to remove the effects of global ocean tides from GRACE data during processing to reduce temporal aliasing into monthly GRACE solutions. These models have typically been derived using data from satellite altimeters such as TOPEX/Poseidon. Therefore the Arctic ocean components of tide models are not constrained by altimetry data, potentially resulting in errors that are likely to alias into monthly GRACE gravity fields at all latitudes. Seven years of GRACE inter-satellite accelerations are inverted to solve for corrections to the amplitude and phase of major solar and lunar ocean tides at latitudes north of 50°N using a mascon approach. The tide model originally applied to our data was FES2004, truncated to maximum degree $l_{max} = 90$. Simulations are performed to verify that our inversion algorithm works as designed. Uncertainty estimates are derived from tidal solutions on land, and by subtracting two independent solutions that each use 3.5 years of data. Features above the noise floor in the M_2, K_1, S_2, and O_1 solutions likely represent errors in FES2004. Errors due to truncating the spherical harmonic expansion of FES2004 are too small, and errors in the land mask model (needed to transform sea surface heights into mass) only affect coastal areas and do not produce similar relative amplitudes for any examined tides. In the oceans north of 50°N, these residuals tend to reduce the FES2004 amplitudes for M_2, K_1, S_2, and O_1. Reductions in the variance of accelerations not used in our inversion suggest that our results can be used to improve GRACE processing.

Citation: Killett,E.,J.Wahr,S.Desai,D.Yuan,andM.Watkins(2011),ArcticOceantidesfromGRACEsatellite accelerations, *J. Geophys. Res.*, *116*, C11005, doi:10.1029/2011JC007111.

1. Introduction

[2] Ocean tides at coastal sites have been studied for over a century using tide gauge data [*Darwin*, 1883; *Doodson*, 1921]. In the 1980s, global ocean tide models [*Schwiderski*, 1980] assimilated tide gauge data to help constrain solutions of tidal hydrodynamic equations. Modern ocean tide models such as FES2004 [*Lyard et al.*, 2006] also rely on satellite altimetry missions such as TOPEX/Poseidon to provide data in deep water, but such data are scarce north of 66°N.

[3] The Earth's gravity field varies with time due to contributions from such things as post-glacial rebound, continental water storage, tides, atmospheric circulation, glacier thinning and non-tidal ocean circulation [*Wahr*, 2007]. Tide models, truncated to some maximum spherical harmonic degree, are routinely used to remove tidal signals from the raw GRACE data during processing. Accurate models of body tides are available [*McCarthy and Petit*, 2004], but ocean tides are more complex due to the irregular drag and resonances caused by bathymetry and coastlines interacting with effects of the Earth's rotation. Residual tidal errors alias into GRACE monthly fields [*Han et al.*, 2005, 2007; *Moore and King*, 2008; *Ray et al.*, 2009; *Egbert et al.*, 2009; *Melachroinos et al.*, 2009; *King et al.*, 2011].

[4] GRACE measures gravity fluctuations using two satellites in the same low (~460 km) polar orbit [*Tapley et al.*, 2004a]. One satellite is ~220 km ahead of the other, with the satellites linked by a microwave ranging system that continuously measures their relative separation distance. A gravity feature affects the leading satellite before the trailing satellite, which changes their separation distance. These data can thus be inverted to obtain the time-variable surface mass distribution. Many GRACE applications describe these mass variations using spherical harmonics, but this research uses mass concentrations ("mascons") [*Luthcke et al.*, 2008] to parameterize variations in surface mass.

[5] We give each mascon several degrees of freedom: a constant, a trend, and amplitudes/phases at frequencies which can represent tides or hydrologic/cryospheric/oceanic (non-tidal) processes. At first, the gravitational force from each mascon is approximated by assuming that all its mass is concentrated at a point at the center of the mascon; this approximation is later relaxed in section 2.2. Our approach solves for these mascon parameters using relative accelerations between the GRACE satellites. Two time derivatives of the range measurements are taken to provide relative acceleration. Figure 1 displays simulated accelerations due to a mascon at 61°N, 36°E which is modeled as a 10 cm thick layer of water spread over a rectangular area 230 km on each

[1]Department of Physics and Cooperative Institute for Research in Environmental Sciences, University of Colorado at Boulder, Boulder, Colorado, USA.
[2]Jet Propulsion Laboratory, California Institute of Technology, Pasadena, California, USA.

Copyright 2011 by the American Geophysical Union.
0148-0227/11/2011JC007111

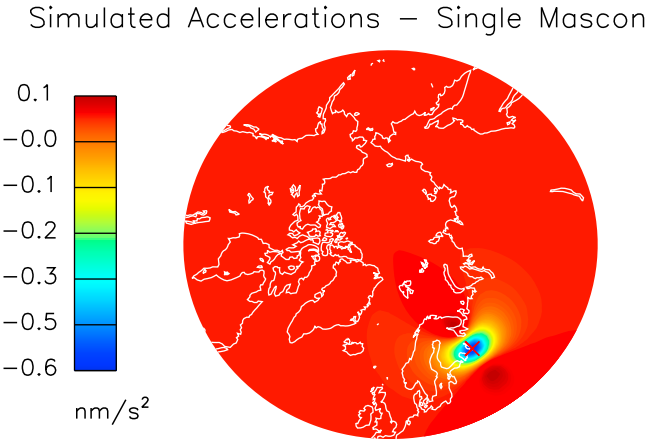

Figure 1. Simulated GRACE accelerations due to a mascon (marked by a red cross) at 61°N, 36°E.

side. The blue feature demonstrates that the GRACE satellites accelerate towards each other when the mascon is between them, while the red features indicate that the satellites accelerate away from each other ~6 times slower when the mascon is north or south of the GRACE pair. The large east-west extent of this "footprint" allows GRACE to recover most diurnal and semi-diurnal tides because successive measurements occur more than twice in each tidal period (at most locations on Earth's surface) which satisfies the Nyquist-Shannon sampling theorem [*Jerri*, 1977].

[6] Differentiation of the range measurements introduces high frequency noise which is smoothed by a Convolution of Rectangle order N (CRN) filter [*Wu et al.*, 2006] at the cost of attenuating signals due to short-scale features. The advantage of using acceleration data is that the observed acceleration at any instant is determined almost completely (see Appendix A) by forces acting on the two satellites at that instant. In contrast, separation distances or velocities are determined by forces acting in the past. An inversion algorithm using accelerations does not need to integrate the mascons' gravitational forces over time, which reduces computation time and hardware requirements.

2. Methodology

[7] Approximately seven years (8 April 2002 to 30 July 2009) of GRACE inter-satellite accelerations [*Case et al.*, 2002] recorded every 5 seconds when the satellites' mid-point is north of 50°N are matched with linearly interpolated positions of each satellite at those times. These accelerations have the dealiasing product AOD1B [*Flechtner*, 2003] subtracted, and are smoothed by a CRN filter with a 20 second cutoff. The complete FES2004 tide model (but without the S_1 fix [*Scharroo*, 2006] or K_2 from FES2002 [*Lyard et al.*, 2006]) is subtracted [*Desai and Yuan*, 2006] after truncation at maximum spherical harmonic degree and order 90.

[8] The observed inter-satellite acceleration is approximately proportional (see Appendix A) to the difference between the accelerations of each satellite projected onto the unit vector ($\hat{\mathbf{n}}$) pointing from GRACE 1 to GRACE 2. Defining $\vec{\mathbf{f}}_{\mathbf{1j}}(t_i)$ as the force per unit satellite mass exerted on GRACE 1 by the j'th mascon at time t_i, Newtonian point mass gravity defines partial derivatives of the i'th acceleration (measured at GRACE positions $\vec{\mathbf{r}}_{\mathbf{1}}(t_i)$, $\vec{\mathbf{r}}_{\mathbf{2}}(t_i)$) with respect to the mass m_j of the j'th mascon (at $\vec{\mathbf{r}}_{\mathbf{j}}$) by

$$\vec{\mathbf{f}}_{\mathbf{1j}}(t_i) = \frac{Gm_j\left(\vec{\mathbf{r}}_{\mathbf{j}} - \vec{\mathbf{r}}_{\mathbf{1}}(t_i)\right)}{\left|\vec{\mathbf{r}}_{\mathbf{j}} - \vec{\mathbf{r}}_{\mathbf{1}}(t_i)\right|^3} \tag{1}$$

$$\frac{\partial a(t_i)}{\partial m_j} = \left(\frac{\vec{\mathbf{f}}_{\mathbf{2j}}(t_i)}{m_j} - \frac{\vec{\mathbf{f}}_{\mathbf{1j}}(t_i)}{m_j}\right) \cdot \hat{\mathbf{n}}. \tag{2}$$

[9] Mass is converted to "equivalent thickness of water" over the mascon using a nominal density of seawater and the area of the mascon. When multiplied by time dependent factors at the epoch of acceleration, equation (2) can represent the acceleration from a mascon's constant, trend, or sinusoidal behavior. The observed accelerations are related [*Tapley et al.*, 2004b] to the mascon parameters by

$$\vec{\mathbf{y}} = \mathbf{H}\vec{\mathbf{x}} + \vec{\epsilon} \tag{3}$$

where $\vec{\mathbf{y}}$ is the observation vector of accelerations corrupted with errors $\vec{\epsilon}$, $\vec{\mathbf{x}}$ is the state vector of mascon parameters with size T = M*P (M mascons, each with P temporal parameters), and $\mathbf{H}$ is the observation-state mapping matrix, filled with values calculated from equation (2). A least squares solution of $\vec{\mathbf{x}}$ in equation (3) is obtained by minimizing a performance index given by the L_2 norm of the errors $\vec{\epsilon} = \vec{\mathbf{y}} - \mathbf{H}\vec{\mathbf{x}}$. This is equivalent to solving

$$\vec{\mathbf{b}} = \mathbf{A}\vec{\mathbf{x}} \tag{4}$$

where $\vec{\mathbf{b}} = \mathbf{H}^T\vec{\mathbf{y}}$ and $\mathbf{A} = \mathbf{H}^T\mathbf{H}$ is the symmetric but indefinite covariance matrix.

[10] The covariance matrix $\mathbf{A}$ is nearly singular, so this ill-posed problem is prone to numerical errors and thus requires regularization. Truncated singular value decomposition [*Press et al.*, 1992] and Gaussian smoothing [*Barmin et al.*, 2001] were tried, but Tikhonov damping [*Aster et al.*, 2005] is faster, requires only a single adjustable parameter, and performs well in simulations (such as those described in section 3). Tikhonov damping is applied by adding a weighted identity matrix to the covariance matrix before using LU decomposition [*Turing*, 1948] to solve

$$\vec{\mathbf{b}} = (\mathbf{A} + \lambda\mathbf{I})\vec{\mathbf{x}}. \tag{5}$$

[11] This addition to the performance index penalizes solutions with large amplitudes, and so tends to smooth the output mascon field. A weighting factor of $\lambda = 20$ was originally subjectively chosen because it produces output which is not too noisy, and does not excessively attenuate continent-scale simulated signals, as discussed in section 3. Later, the accelerations implied by the mascon field are subtracted from verification accelerations (see section 4.2) not used in the inversion. The relative variance reduction of the verification accelerations reaches a maximum when λ is set between 19 and 21, thus supporting our original choice of $\lambda = 20$.

[12] One mascon is placed at the North Pole and others form concentric circles around it with nearly equal areas, though small latitude-dependent deviations exist due to the

need to have an integer number of grid points at each latitude. These areas should be similar because each mascon's mass (in kg) is converted to the equivalent thickness of water. Placing this conversion in **A** avoids numerical problems inherent to large differences in the magnitudes of the observation and state vectors.

[13] The conversion from mass to water thickness depends on the assumed density of water, so errors in that density affect the accuracy of the inverted mascon field relative to tide gauges. Here, water density is assumed to be a uniform 1035 kg/m^3 because tides move the entire water column which has a more stable temperature and salinity than surface water, and because the effects of a laterally [*Steele and Ermold*, 2007] and temporally [*Wang et al.*, 2010] varying density are not likely to rise above the current GRACE noise floor. However, future studies may need to account for local variations and small annual density fluctuations [*Willis et al.*, 2008] that would otherwise modulate the estimate of water thickness.

[14] This research does not correct for the fact that GRACE can not detect changes in the Earth's center of mass relative to the geometric center of the Earth. This problem is alternatively described as an inability to reconstruct the degree 1 spherical harmonic terms of the Earth's surface mass distribution using GRACE data alone [*Swenson et al.*, 2008].

[15] The GRACE observations are sensitive to the sum total of the mass displacements due to ocean tides and displacements in the solid Earth due to the load of ocean tides. Our results report this total contribution, but expressed as the height of the effective water thickness. Future work should include approaches to separate the two contributions to enable recovery of the ocean tide height with respect to the ocean bottom. Possible approaches might be analogous to those used to separate the ocean and load tide heights from satellite altimetry observations [*Cartwright and Ray*, 1991], except in the case of GRACE considering that the observations are of mass rather than sea surface height. Doing so would facilitate appropriate comparisons to tide gauge observations.

[16] Source code is available at http://emmykillett.com.

2.1. Zone of Influence

[17] Summing the contributions of all accelerations for every entry in the covariance matrix would take months on a typical desktop computer. To increase speed, each acceleration is only allowed to contribute to a mascon solution, for mascons lying within a certain distance (measured from the mascon center to the projection of the satellites' midpoint onto a spherical Earth). This "zone of influence" moves with the satellites and is different for each acceleration measurement. Thus in principle it is necessary to calculate the distances from the satellites' midpoint to all mascons at all times to determine which mascons lie within the zone of influence. Because there are millions of acceleration measurements, this strategy would not provide a significant speedup.

[18] However, each acceleration value can be matched to the closest mascon (of which there are usually merely thousands rather than millions) and the zone of influence is then determined from values that have been pre-calculated using that mascon's position, rather than determined directly from the position of the satellites' midpoint. This approximation reduces the number of required calculations by a factor of ~10^3 and introduces negligible errors because any omitted mascons are already far away from the acceleration measurement in question.

[19] The algorithm's only parameter is the zone radius; smaller values dramatically reduce the computation time at the cost of increasing error by ignoring mascons that contribute substantially to the measured accelerations. The simulations in section 3 and real inversions in section 4 use a zone radius of 2050 km, which introduces relative errors in the output mascon field that are less than 10% of the maximum mascon value. The simulated accelerations in Figure 1 suggest that choosing a zone radius too small to cover the significantly non-zero portion of that map will increase error, which is observed in experiments not shown here.

2.2. Support Grid Points

[20] One drawback of using Newtonian point mass gravity is that real tides are distributed over the surface of the Earth rather than concentrated as geometric points. This inaccuracy is sometimes avoided by modeling the mascons as uniform disks, and computing their gravitational signatures as spherical harmonic expansions. These infinite expansions converge on a gravitational solution for a distributed mass. But truncating at a finite number of terms for numerical computation introduces non-local errors (i.e. creates an effective non-zero mass distribution outside the mascon).

[21] These errors can be circumvented by placing the point masses close enough together that GRACE is not sensitive enough to distinguish them. Unfortunately, this approach requires more memory than our computers have available because the size of the covariance matrix scales as the square of the number of grid points, which scales as the inverse square of the grid spacing.

[22] Our solution is to use support grid points to account for the distributed nature of the genuine water mass while avoiding non-local errors. Each main grid point has a set of support points associated with it. They evenly fill the space between main grid points with arbitrary spatial density. For example, in Figure 2 the main grid points are shown in black and the colors of the support points indicate which main grid point they are associated with.

[23] The support points' gravitational effects are summed together (weighted according to surface area so each support point has the same sea surface height as the main grid point) with the main grid point to produce a single entry in the covariance matrix. The mass which was previously assumed to be concentrated at the main grid point is now distributed over the support points so that the equivalent thickness of water is spread more uniformly over the area of the mascon. Adding support points does not increase memory requirements, but also does not increase the spatial resolution of the resulting map.

[24] The centers of the mascons are separated by about 230 km, and each mascon used in section 4 has 24 support points. Expanding a 230 km diameter spherical cap's gravity into harmonics [*Farrell*, 1972] up to degree 200 converged to within 0.8% of that due to 24 support points.

3. Simulations

[25] To test the inversion algorithm, synthetic mascon fields are created for two separate simulations. The centers of these mascons (indicated by red dots in Figure 3) are

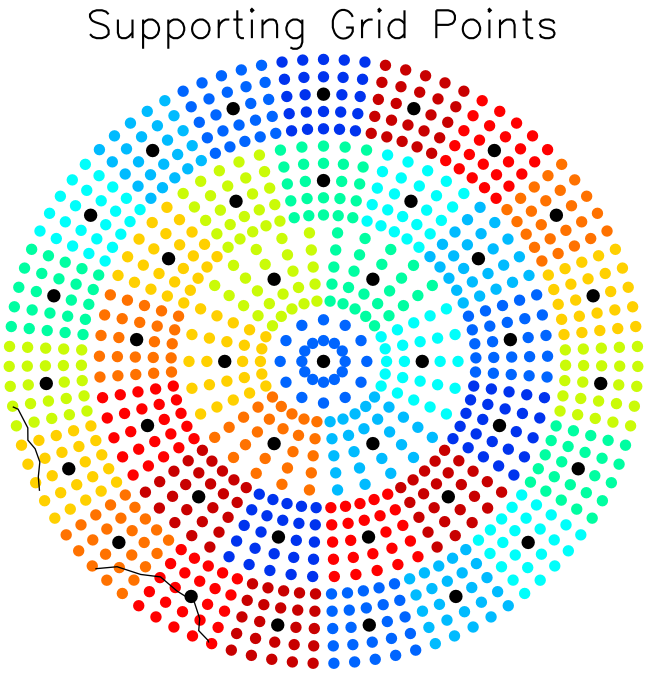

Figure 2. Main grid points are shown in black, separated by about 230 km. Each main grid point is associated with 24 color-coded support points.

separated by about 230 km and cover the Earth north of 50°N latitude. Each set of simulated mascon fields includes a 10 cm/year trend over land mascons (not shown) with no trend over ocean mascons, in addition to the M_2 and K_1 sine and cosine patterns shown in Figure 3. In this context, "cosine" means the coefficient of $\cos(\omega t)$ where t = 0 at J2000. These are upward-continued using Newtonian gravity to calculate the relative accelerations caused by those mascon fields as measured by GRACE. The actual positions of the GRACE satellites over seven years are used in this upward continuation process. The resulting synthetic accelerations are then inverted using the regularized least squares fit procedure described in section 2 to simultaneously deduce the implied surface mascon time dependencies for the secular trend as well as the M_2 and K_1 sine and cosine coefficients. This test is designed to assess the effects of regularization, and nothing else.

[26] In both simulations, the input M_2 and K_1 sine maps are identical and both input cosine maps are zero. Output sine maps for M_2 and K_1 in both simulations are so similar that only the maps for M_2 are shown. They demonstrate that regularization does not appreciably attenuate continental-scale signals. Since cosine inputs are zero, the cosine solutions are presumed to be leakage errors from other inputs. The K_1 cosine map errors are ~15% of the maximum input sine amplitude, largest at the North Pole and ~20 times larger than errors in M_2. When the secular trend is removed from the input, the errors in K_1 are no longer significantly larger than those in M_2, suggesting that the simulated K_1 North Pole anomaly results from interactions between K_1 and the trend when regularization is applied, possibly related to the long alias period of K_1.

[27] In these simulations, the Newtonian gravity algorithm is applied twice, once for upward continuation from the input mascon fields to the synthetic acceleration time series, and once for the inversion from the acceleration time series to the output mascon fields. Instrumentation noise is not included in the simulated data, but the same regularization used with noisy real data is applied.

[28] The resolution is determined by inverting the accelerations due to a single simulated non-zero mascon shown in Figure 1. The resulting mascon field (not shown) blurs the single point into a broader feature with a half-width of ~300 km and attenuates the peak amplitude more than in the continental scale simulations. The mascon spacing of ~230 km is chosen because it is small enough not to constrain the resolution but large enough so the resulting covariance matrix fits into the computer's memory.

4. Real Data Inversions

[29] Real acceleration data generated at the Jet Propulsion Laboratory (JPL) are inverted using the regularized least squares fit procedure described in section 2 to produce mascon fields for tides M_2, K_1, S_2, and O_1. All parameters are inverted simultaneously over the entire globe north of 50°N, along with a constant, secular trend, and semi-annual and annual periods (not shown).

[30] In Figures 4a, 4e, 5a, and 5e are FES2004 M_2, K_1, S_2, and O_1 amplitudes; note that the FES2004 maps have (saturated) color scales that are much larger than the other maps. Corresponding mascon amplitude maps from the inversion of real data follow, with the average amplitude on land noted (see section 4.1). Next are maps showing the changes in FES2004's amplitudes when the inverted residual estimates are added to the original FES2004 model. On the right are amplitudes of the differences between two independent mascon solutions each using 3.5 years of independent data.

[31] For deep ocean tides, FES2004 relies primarily on TOPEX/Poseidon altimetry data which do not extend north of 66°N. One might expect that mascon solutions should reveal systematically larger residual tidal amplitudes north of 66°N versus south of 66°N, which is not the case for any examined tides. In the oceans north of 50°N, the mascon solutions tend to reduce the FES2004 amplitudes for M_2, K_1, S_2, and O_1.

[32] The GRACE-observed difference between FES2004 and its expansion to degree 90 (the maximum degree used when removing FES2004 from the raw GRACE data) is called truncation error. The difference between the land mask used in GRACE processing and the actual coastlines is called the land mask error.

[33] Truncation errors are simulated by subtracting the $l_{max} = 90$ spherical harmonic expansion of FES2004 from the original FES2004 model. These truncation errors are upward-continued to GRACE accelerations, then inverted using the same procedure that is applied to the real accelerations. The inverted truncation errors for M_2 and K_1 are well below the ~1 cm GRACE noise floor determined in section 4.1.

[34] Because tide models give sea surface height but GRACE senses mass, the GRACE tide correction involves a summation over all non-zero FES2004 grid points. Thus, it is important that FES2004 give sea surface height everywhere in the ocean and does not give a non-zero sea surface height anywhere on land. Errors in the FES2004 land mask could play a larger role in narrow inlets such as Hudson Strait and the Canadian archipelago, but they should also produce

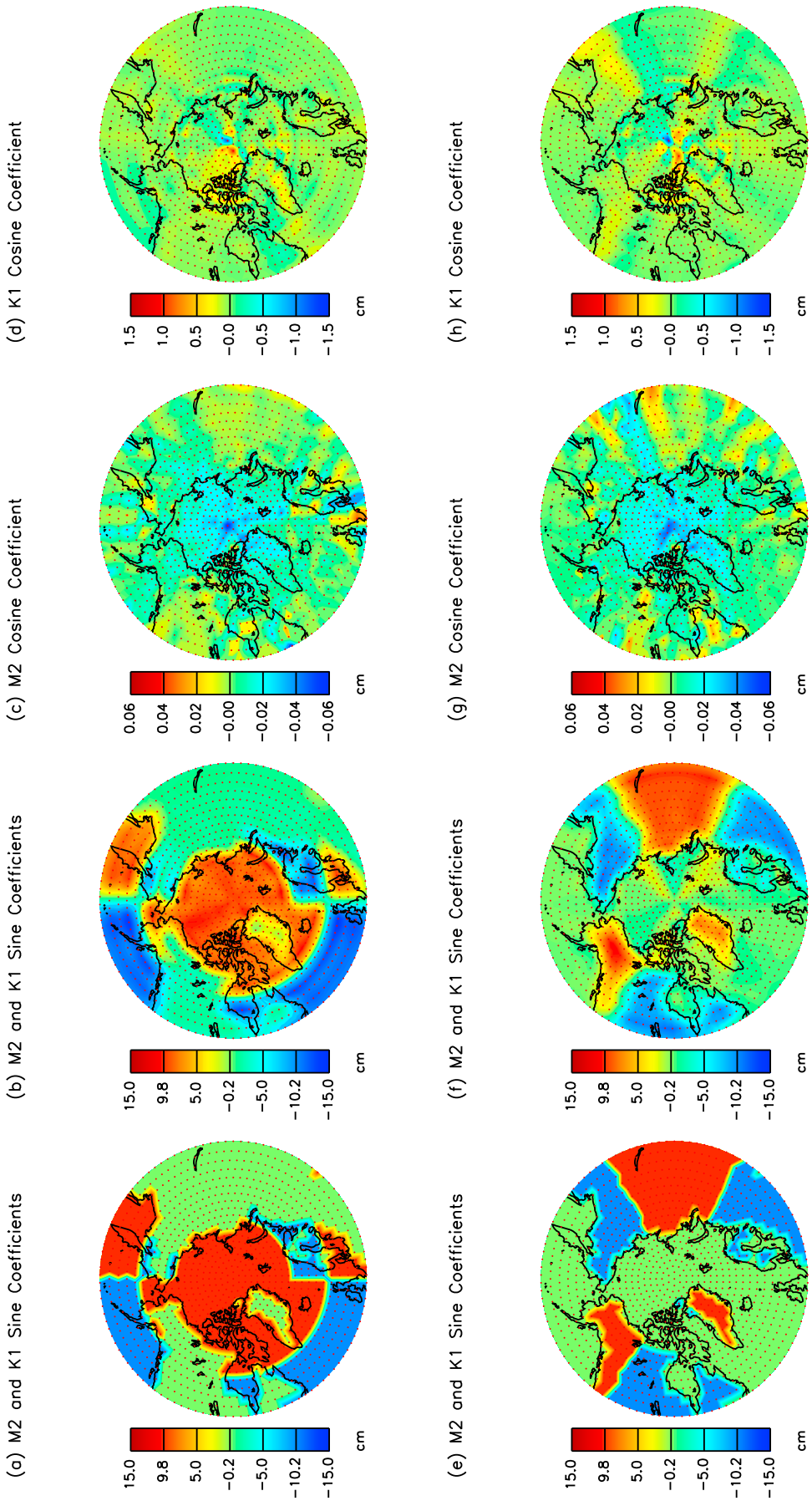

Figure 3. Two separate simulations: (a and e) Inputs. Both M_2 and K_1 inputs are identical in each simulation, cosine inputs are also zero, and a 10 cm/yr trend over land is included as input. (b and f) Sine outputs for both M_2 and K_1 because they are so similar. (c and g) Small M_2 cosine outputs. (d and h) Larger K_1 cosine outputs, which are leakage errors from other inputs.

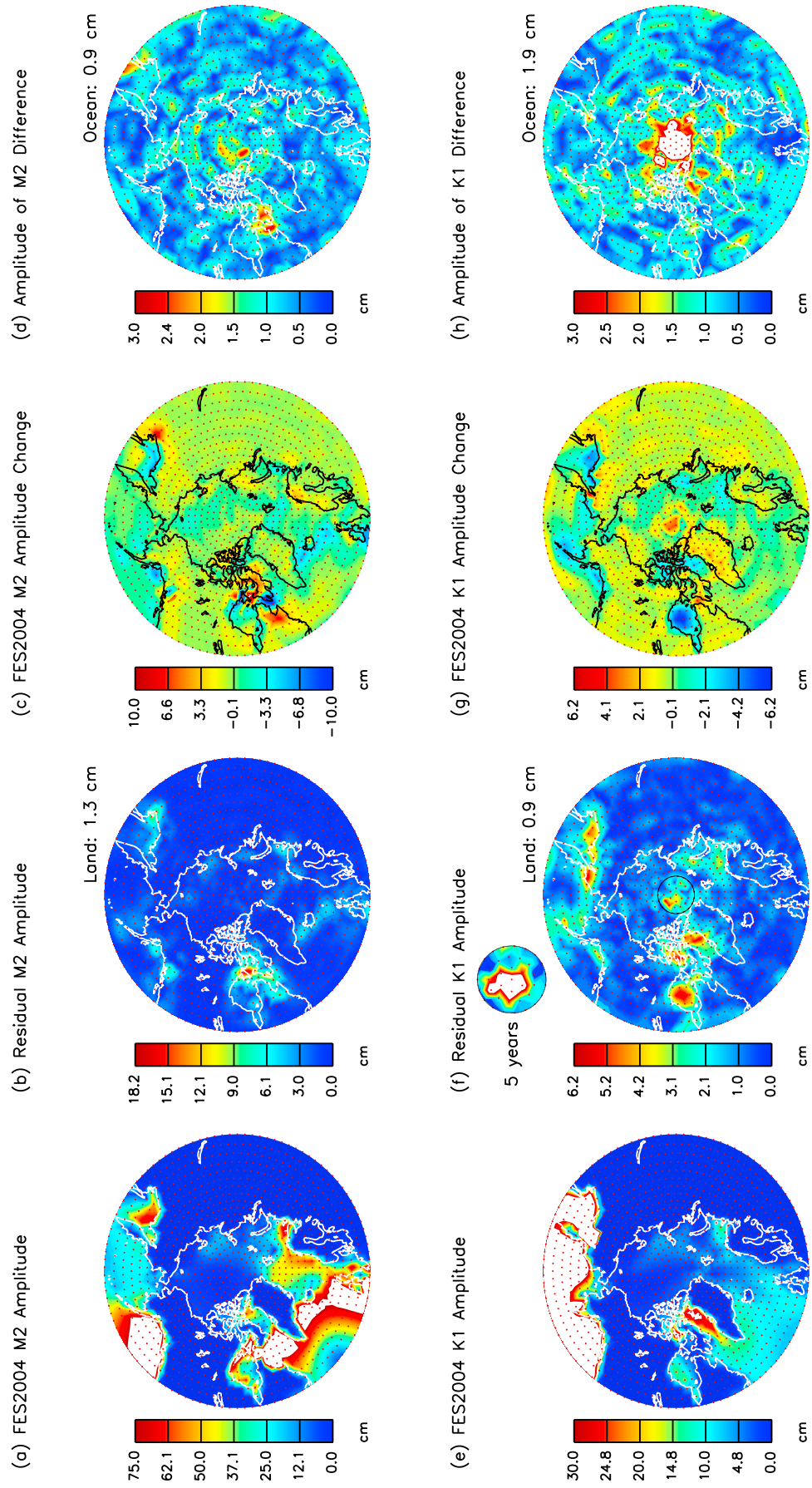

Figure 4. (a and e) FES2004 M_2 and K_1 amplitudes with large, saturated color scales. (b and f) Corresponding mascon amplitude maps from the inversion of real data, with smaller color scales and average land amplitudes. Note that the K_1 North Pole anomaly in Figure 4f is much larger when only 5 years of data are inverted (inset, with a maximum amplitude of 9.6 cm saturating the color scale). (c and g) The changes in FES2004's amplitudes when the inverted residual estimates are added to the original FES2004 model. (d and h) Amplitudes of the differences between two mascon solutions each using 3.5 years of independent data.

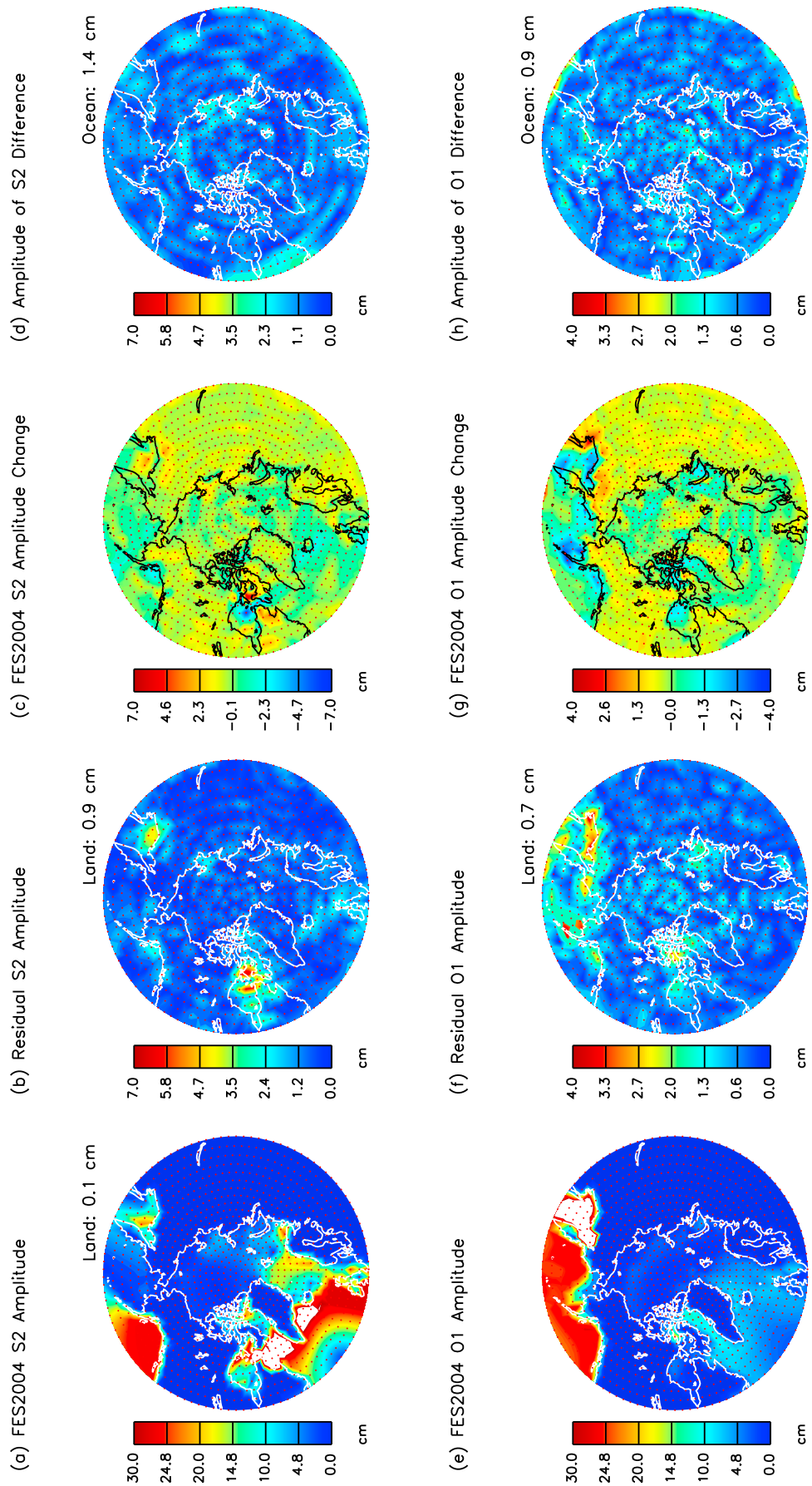

Figure 5. (a and e) FES2004 S_2 and O_1 amplitudes with large, saturated color scales. (b and f) Corresponding mascon amplitude maps from the inversion of real data, with smaller color scales and average land amplitudes. (c and g) The changes in FES2004's amplitudes when the inverted residual estimates are added to the original FES2004 model. (d and h) Amplitudes of the differences between two mascon solutions each using 3.5 years of independent data.

relative errors of similar magnitude for different tides in the same location. This correlation is not observed; for instance the K_1 residual features in the Canadian archipelago and Baffin Bay do not have corresponding M_2 residual features in the same places, even though the FES2004 amplitudes for both tides are appreciable in those locations.

4.1. Uncertainty Estimates

[35] The mascon fields from the inversions tend to have much larger tidal amplitudes in the ocean than on land. Land tides at mascons that do not intersect the ocean (colored green in Figure 3a) are assumed to be due to some combination of truncation errors in the expansion of FES2004, errors in body tide modeling, processing and instrumentation errors in the GRACE data, aliasing, leakage from short-period non-tidal ocean signals, aliased hydrologic/cryospheric processes, errors in the ocean loading models removed from the raw data, and errors introduced by neglecting the non-line-of-sight acceleration terms (see Appendix A). These land tide solutions can be used to determine error estimates for the ocean tide solutions by defining the true tidal signal and the observed tidal estimate at a given point on the Earth's surface

$$T_{true}(t) = (a)\cos(\omega t) + (b)\sin(\omega t) \tag{6}$$

$$T_{obs}(t) = (a + \delta a)\cos(\omega t) + (b + \delta b)\sin(\omega t). \tag{7}$$

The corresponding true and observed tidal amplitudes are

$$A^2_{true} = a^2 + b^2 \tag{8}$$

$$A^2_{obs} = (a + \delta a)^2 + (b + \delta b)^2. \tag{9}$$

[36] Given many GRACE time series of length 7 years, and assuming the errors δa and δb are drawn from a Gaussian distribution with zero mean (and so are uncorrelated with the true signal and with each other), implies a statistical mean observed squared amplitude of

$$\left(A^2_{obs}\right)_{mean} = A^2_{true} + var(\delta a) + var(\delta b). \tag{10}$$

[37] Note that the statistical mean observed squared amplitude is always biased positively even by errors with zero mean due to the nonlinear relationship between the amplitude and the cosine/sine coefficients. A_{true} should be zero on land, so the average value of A_{obs} on land is an estimate of $\sqrt{var(\delta a) + var(\delta b)}$. Assuming that land and ocean mascons are affected by similar noise processes, and thus have similar values of $\sqrt{var(\delta a) + var(\delta b)}$, any ocean mascons with $A_{obs} \leq \sqrt{var(\delta a) + var(\delta b)}$ are unlikely to be good representations of A_{true}. Each inverted tidal amplitude's average land tide value is noted in Figures 4 and 5, and can serve as a rough error estimate for the tidal solution over the ocean.

[38] A second uncertainty estimate is derived from the difference between two independent solutions, each using 3.5 years of data. This estimate has the spatial pattern shown in Figures 4d, 4h, 5d, and 5h along with an ocean average to compare with the previously described land tide average. The ocean tide difference using 3.5 years of data likely overestimates the uncertainty in the 7 year solution. This is especially true for K_1 at the North Pole (see section 4.4), and when the North Pole anomaly is removed from Figure 4h, the average K_1 ocean difference drops from 1.9 cm to 1.2 cm. These estimates (as well as those by *Han et al.* [2007, 2010]) support a ~1 cm uncertainty, though the difference maps reach 2–3 cm in some places. Estimating uncertainty using two independent solutions does not assume that oceanic noise is equal to or smaller than land noise, unlike the uncertainty estimate derived from land mascons.

4.2. Noise Reduction

[39] The accelerations implied by the mascon fields are guaranteed to reduce the variance of GRACE accelerations used in the inversion. Some GRACE accelerations are withheld from another inversion for a more independent test of the accuracy of the mascon fields. A second acceleration time series with approximately five years of data (8 April 2002 to 3 June 2007) is used in this section because it was filtered with a 50 second cutoff period, and is thus less noisy than the 20 second data set. The first 80% of the accelerations are used to solve for tides and a non-tidal component consisting of a constant, trend, and semi-annual and annual amplitudes. The last 20% of the data are reserved to verify that the inverted mascons reduce the variance of acceleration values not used in the solution.

[40] The accelerations due to the non-tidal part of the solution are subtracted from the original accelerations, then the additional reduction in variance due to the tides is calculated. The reduction due to tides is calculated separately for ocean tides (defined as tides at mascons with at least some ocean) and land tides (tides at mascons with no ocean; see Figure 3a). Each variance reduction in Table 1 is calculated separately for accelerations used in the inversion and those reserved for verifications.

[41] In 100 Monte Carlo tests, the accelerations due to the ocean tides are subtracted from a random time series of accelerations with mean and variance equal to the GRACE verification accelerations after the non-tidal accelerations have been subtracted. The ocean tides never reduce the variance but always increase it by at least 1.2%. For comparison, Table 1 shows that ocean tides reduce the verification GRACE variance (after non-tidal subtraction) by 1.46%, corresponding to an RMS reduction of 0.03 nm/s^2.

[42] The ocean tides reduce the variance of the verification accelerations by 1.46%, which is 78% as much as their 1.88% reduction of the variance of inverted accelerations. The land tides, however, reduce the variance of the verification accelerations by 0.17%, which is 45% as much as their 0.38% reduction of the variance of inverted accelerations. This suggests that land tides are noisier than ocean tides, but also shows that land tides are not entirely random (otherwise they would not reduce the variance at all). Thus, roughly 45% (by variance) of the land tide estimate may represent mismodeled ocean loading, mis-modeled body tides, or aliased hydrological signals which would also appear in the verification accelerations.

4.3. Power Spectra

[43] A second acceleration time series, filtered with a 50 second cutoff period, is sent through a Fast Fourier Transform

Table 1. Variance Reduction Due to Tides[a]

Tide	Surface Sum (kg^2)	Acceleration Variance Reduction: Inversion (%)	Verification (%)	Decrease (%)
Ocean	2.22×10^{27}	1.88	1.46	77.8
Land	3.99×10^{27}	0.38	0.17	44.5

[a]Surface sums are computed separately for ocean and land mascons by summing the squares of all the tidal cosine and sine coefficients in kg on the Earth's surface; these residual tidal estimates reduce the variance of GRACE accelerations used in the inversion, and accelerations reserved for verification; the verification reduction is then divided by the inversion reduction to obtain the normalized decrease shown in the fifth column. Note that the variance reduction due to land tides decreases more than ocean tides when comparing the variance reduction of verification accelerations to accelerations used in the inversion.

to obtain the power spectra in Figure 6a. Accelerations used in the inversion and those reserved for verification both yield spectra with one sharp peak at 0.003 Hz and a second broader peak centered at 0.02 Hz. The second peak has a period of 50 seconds because that is the period at which the CRN filter starts to remove accelerometer (and other instrumentation) noise. The verification time series has more power than the inversion time series only when the last 20% of the data are used for verification; this difference is not reproduced when any other segment of equal size is used for verification.

[44] A synthetic spectrum using ten tides in FES2004 ($M_2, K_1, K_2, O_1, P_1, S_2, N_2, Q_1, M_f, M_m$) is shown in Figure 6b. The synthetic and real noise spectra have the first peak in common, but the lack of a second peak in the synthetic spectrum suggests that power at those frequencies in the real data spectrum probably is not caused by tides. Note that these power spectra are more closely related to the spatial pattern of the tides than to their tidal periods because the GRACE orbital period of ~90 minutes is much shorter than even semi-diurnal tidal periods. The real data inversions in section 4 are therefore presumably attempting to fit the signal comprising the first peak. To test this, the real data inversions are upward continued and subtracted from the original acceleration time series. The relative variance reductions due to the mascons are shown in Figures 6c and 6d.

[45] Figures 6c and 6d suggest that ~90% of the noise reduction in the first peak can be attributed to the non-tidal parameters. The remaining noise reduction is due to ocean mascons' oscillations at tidal frequencies M_2, K_1, S_2, and O_1. In addition to the noise sources listed in section 4.1, residual noise in the first peak may be due to errors in other tides, interannual signals, accelerating mass changes such as those in Greenland, year-to-year fluctuations in the annual amplitudes, mis-modeled short-period atmospheric and oceanic processes, aliased long period non-tidal ocean signals, or signals caused by ocean tides south of 50°N. The reductions shown in Figures 6c and 6d increase at frequencies around 0.04 Hz due to roundoff errors caused by dividing by the spectra in Figure 6a which approach zero around that frequency.

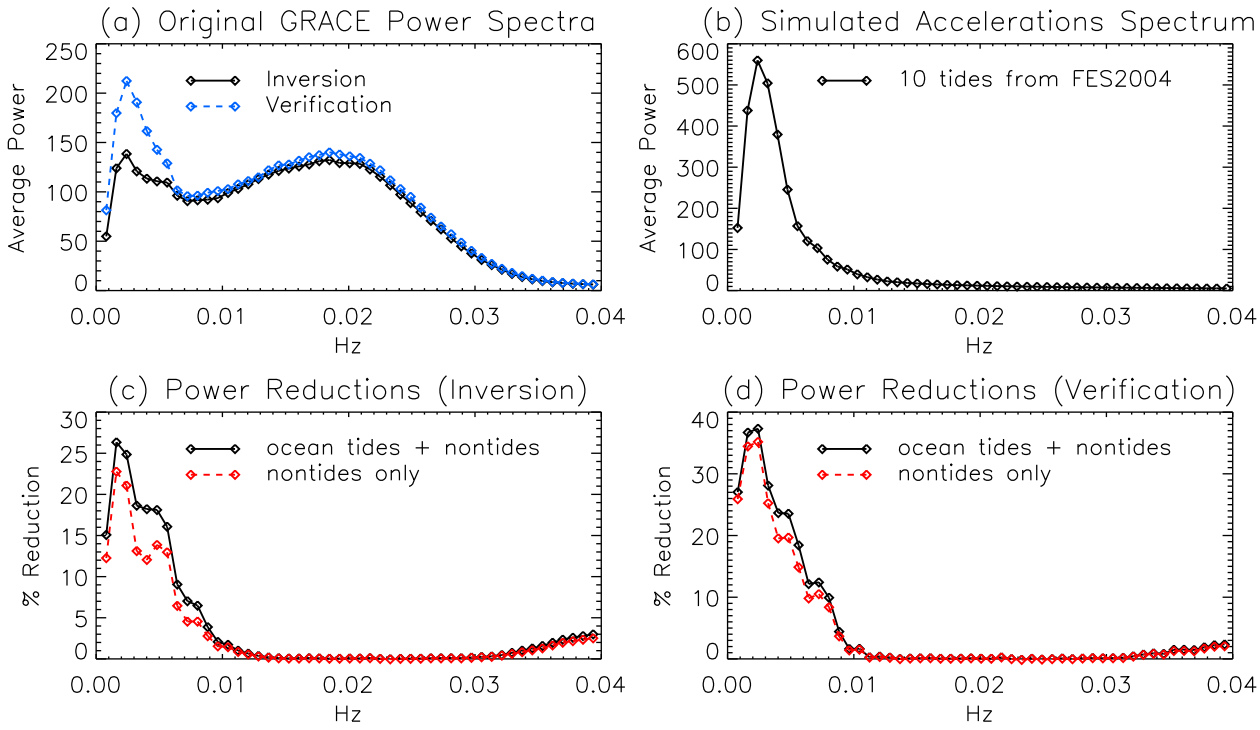

Figure 6. (a) GRACE accelerations filtered with a 50 second cutoff period are split into two segments: one (solid black curve) used to invert for mascon estimates and another (dashed blue curve) used only for verification, then sent through a Fast Fourier Transform to obtain power spectra. (b) A synthetic GRACE spectrum using ten tides in FES2004 ($M_2, K_1, K_2, O_1, P_1, S_2, N_2, Q_1, M_f, M_m$). (c and d) The relative variance reductions due to upward-continued mascon estimates for both inversion and verification accelerations. The solid black curves include ocean tides and nontidal parameters, while the dashed red curves only include nontidal parameters.

4.4. The K_1 North Pole Anomaly

[46] The K_1 inversions in Figures 3h (simulated data) and 4f (real data) reveal an anomaly at the North Pole. At latitudes south of the turning latitude (89°N) GRACE samples the K_1 tide twice during each tidal period on the ascending/descending passes. Because K_1 is a diurnal tide, the ascending and descending passes measure phases that are nearly 180° apart, which reduces aliasing [*Ray and Luthcke*, 2006; *Han et al.*, 2010]. At the turning latitude, however, the tide is only measured with maximum sensitivity once during each period because GRACE's sensitivity is strongest directly underneath the GRACE midpoint and because the K_1 forcing potential is stationary in inertial space. If the GRACE orbit did not precess, it would always sample the same phase of K_1 at the turning latitude, yielding an infinitely long alias period. However, the GRACE orbit does slowly precess [*Knudsen and Andersen*, 2002], which results in K_1's finite ~7.5 year alias period [*Ray and Luthcke*, 2006] in the GRACE data at the turning latitude.

[47] As the data span has lengthened from five to seven years, the K_1 North Pole anomaly has shrunk in amplitude and geographical extent (see inset in Figure 4f). In contrast, at all points on the globe K_2 should display the same behavior that K_1 does at the pole because K_2's semi-diurnal symmetry means that even at points far from the pole, ascending and descending passes both measure the same phase, which does not satisfy the Nyquist-Shannon sampling theorem. Inversions of real data (not shown) confirm that K_2 is unstable over the entire region north of 50°N even with seven years of GRACE data.

[48] The FES2004 solution for every tidal constituent except S_1 has an irregularly shaped region ~40 km in diameter, centered on the North Pole, that is treated as land by the model, in the sense that the tides are not modeled there. However, this hole is independent of the data span and should affect M_2 more than K_1 because M_2 has a larger amplitude around the hole, so the hole probably is not contributing significantly to the North Pole anomaly in K_1.

5. Conclusions

[49] We have used seven years of GRACE acceleration data to solve for M_2, K_1, S_2, O_1, and (not shown) P_1 and K_2. The solutions look plausible, except for K_1 near the North Pole and K_2 in at least the entire region north of 50°N, limitations which are likely due to aliasing. Ocean tides reduce the variance of accelerations not used by the inversion nearly as well as they reduce the variance of accelerations used in the inversion. This suggests that the ocean mascon tidal solutions can improve GRACE processing. The variance reduction due to land tides drops off more sharply when applied to accelerations not used in the inversion. The land tides are used as uncertainty estimates which confirm the ~1 cm uncertainty derived by subtracting two independent solutions based on 3.5 years of data. Solutions with improved accuracies might be obtained by inverting GRACE data using code which accounts for non-line-of-sight acceleration terms (see Appendix A) and simultaneously solves for GRACE's orbital parameters as well as surface mascons, such as JPL's MIRAGE software.

[50] Truncation errors, land mask errors and errors in the assumed density of seawater are too small to account for residual features that rise above the noise floor. These features are probably caused by errors in the FES2004 amplitudes and phases. For instance, seasonal ice cover in Hudson Bay hinders altimeters and could contribute to the K_1 residual feature there because FES2004 uses ERS crossover data in Hudson Bay, and the alias period of K_1 in the ERS data is 365.25 days [*Ray et al.*, 2003]. Adding the residual estimates to FES2004 indicates that FES2004 overestimates the K_1 amplitude by up to 50% in Hudson Bay and north of Siberia. In fact, the signs of the residual estimates suggest that FES2004 amplitudes for M_2, K_1, S_2, O_1, and P_1 tend to be too large in many regions throughout the oceans north of 50°N. Exceptions are M_2 and S_2 in Foxe Basin, K_1 in Hudson Strait, and S_2 in the Sea of Okhotsk.

[51] All large M_2 residual features are spatially correlated with large amplitudes in the original FES2004 M_2 model, such as those in Hudson Strait, southeast of Greenland, northeast of Scandinavia, off the coast of Alaska, and in the Sea of Okhotsk. Similarly, most large K_1 residual features are spatially correlated with large amplitudes in the original FES2004 K_1 model, such as those in Hudson and Baffin Bays, the Canadian archipelago, northeast of Scandinavia, and in the Sea of Okhotsk. The only exception is the ~3 cm K_1 residual feature in Hudson Strait, where FES2004 shows a K_1 amplitude of only ~2 cm. Residual features in the S_2 and O_1 inversions are also correlated with large amplitudes in their respective FES2004 maps. These correlations suggest that errors in FES2004 are proportional to tidal amplitude, which would not be the case for a tide model based purely on altimetry data.

[52] Large features in the residual tidal estimates could be associated with poor coverage of tide gauge observations assimilated by FES, or large errors in nearby tide gauges. Flaws in the bathymetry model used by FES2004 might also play a role, especially in shallow waters like Hudson Strait. The residual estimates are not larger north of the TOPEX/Poseidon turning latitude of 66°N. FES2004 may be overcoming this lack of coverage with its hydrodynamic modeling and its assimilation of Arctic tide gauge data and crossover points from the ERS satellite which has an ~81°N turning latitude.

[53] Future work will be necessary to use the GRACE-derived tidal corrections to improve tide gauge comparisons, likely because point measurements from tide gauges are more sensitive to local variations in tidal amplitudes and phases than GRACE [*Han et al.*, 2010], and also because this work neglects ocean loading.

Appendix A

[54] Let $\vec{\mathbf{p}} = \vec{\mathbf{p_2}} - \vec{\mathbf{p_1}}$ be the separation vector between the GRACE satellites. The distance between the satellites is $p = |\vec{\mathbf{p}}| = \vec{\mathbf{p}} \cdot \hat{\mathbf{n}}$ where $\hat{\mathbf{n}}$ is the unit vector pointing from GRACE 1 to GRACE 2. The observed satellite-to-satellite acceleration is $a = \frac{d^2}{dt^2}p$ which can be expanded as

$$a = \ddot{\vec{\mathbf{p}}} \cdot \hat{\mathbf{n}} + \dot{\vec{\mathbf{p}}} \cdot \dot{\hat{\mathbf{n}}} \tag{A1}$$

because $\vec{\mathbf{p}} \cdot \hat{\mathbf{n}} = 0$.

[55] The separation vector $\vec{\mathbf{p}}$ is affected by many factors including the centripetal acceleration of the GRACE orbits, spatial variations in the Earth's static gravity field, non-tidal

oceanic and atmospheric circulation, and body and ocean tides. JPL subtracts changes in $\vec{\mathbf{p}}$ due to models of each of these factors; this research examines changes in $\vec{\mathbf{p}}$ due to errors in the FES2004 ocean tide model. Let

$$\vec{\mathbf{p}} = \vec{\mathbf{p}}_0 + \delta\vec{\mathbf{p}} \tag{A2}$$

where $\delta\vec{\mathbf{p}}$ are changes due to errors in FES2004 and $\vec{\mathbf{p}}_0$ are changes due to all other factors, where $\delta\vec{\mathbf{p}} \ll \vec{\mathbf{p}}_0$. Similarly,

$$\hat{\mathbf{n}} = \hat{\mathbf{n}}_0 + \delta\hat{\mathbf{n}}. \tag{A3}$$

[56] Inserting equations (A2) and (A3) into equation (A1) yields

$$a = \left(\ddot{\vec{\mathbf{p}}}_0 + \delta\ddot{\vec{\mathbf{p}}}\right) \cdot \left(\hat{\mathbf{n}}_0 + \delta\hat{\mathbf{n}}\right) + \left(\dot{\vec{\mathbf{p}}}_0 + \delta\dot{\vec{\mathbf{p}}}\right) \cdot \left(\dot{\hat{\mathbf{n}}}_0 + \delta\dot{\hat{\mathbf{n}}}\right). \tag{A4}$$

[57] When one expands equation (A4), terms that are the product of one δ with another δ are small enough to be neglected. Furthermore, JPL has already subtracted terms without any δ, so the remaining first-order effect of ocean tide errors is:

$$\delta a = \delta\ddot{\vec{\mathbf{p}}} \cdot \hat{\mathbf{n}}_0 + \ddot{\vec{\mathbf{p}}}_0 \cdot \delta\hat{\mathbf{n}} + \delta\dot{\vec{\mathbf{p}}} \cdot \dot{\hat{\mathbf{n}}}_0 + \dot{\vec{\mathbf{p}}}_0 \cdot \delta\dot{\hat{\mathbf{n}}}. \tag{A5}$$

[58] In the derivation of equation (2) in section 2, only the first term in equation (A5) is included because the other terms are presumed to be negligible at tidal frequencies, and because the other terms depend on forces applied to the satellites in the past.

[59] **Acknowledgments.** Thanks to the FES2004 authors for their model and sharing the code, Wenwen Lu and Sung Byun for providing the GRACE acceleration data, Fan-Chi Lin for suggestions that led to the zone of influence algorithm, Richard Ray for insight into the origin of the North Pole anomaly in K_1, Sean Swenson for writing the first version of the IDL graphics code, and Shin-Chan Han and two anonymous reviewers for helpful corrections. This work is supported by NASA grant NNX08AF026 and JPL contract 1390432 to the University of Colorado. This work was performed, in part, at the Jet Propulsion Laboratory, California Institute of Technology, under contract with the National Aeronautics and Space Administration. Source code is available at http://emmykillett.com.

References

Aster, R., C. Thurber, and B. Borchers (2005), *Parameter Estimation and Inverse Problems*, Academic, Amsterdam.

Barmin, M., M. Ritzwoller, and A. Levshin (2001), A fast and reliable method for surface wave tomography, *Pure Appl. Geophys.*, *158*(8), 1351–1375.

Cartwright, D., and R. Ray (1991), Energetics of global ocean tides from Geosat altimetry, *J. Geophys. Res.*, *96*(C9), 16,897–16,912.

Case, K., G. Kruizinga, and S. Wu (2002), GRACE level 1B data product user handbook, *JPL Publ., D-22027*, NASA Jet Propul. Lab., Pasadena, Calif.

Darwin, G. (1883), Reports of a committee for the harmonic analysis of tides, Br. Assoc. for the Adv. of Sci., York, U. K.

Desai, S. D., and D.-N. Yuan (2006), Application of the convolution formalism to the ocean tide potential: Results from the Gravity Recovery and Climate Experiment (GRACE), *J. Geophys. Res.*, *111*, C06023, doi:10.1029/2005JC003361.

Doodson, A. (1921), The harmonic development of the tide-generating potential, *Proc. R. Soc. London, Ser. A*, *100*(704), 305–329.

Egbert, G. D., S. Y. Erofeeva, S.-C. Han, S. B. Luthcke, and R. D. Ray (2009), Assimilation of GRACE tide solutions into a numerical hydrodynamic inverse model, *Geophys. Res. Lett.*, *36*, L20609, doi:10.1029/2009GL040376.

Farrell, W. (1972), Deformation of the Earth by surface loads, *Rev. Geophys.*, *10*(3), 761–797.

Flechtner, F. (2003), AOD1B product description document, GRACE project documentation, pp. 327–750, NASA Jet Propul. Lab., Pasadena, Calif.

Han, S.-C., C. K. Shum, and K. Matsumoto (2005), GRACE observations of M_2 and S_2 ocean tides underneath the Filchner-Ronne and Larsen ice shelves, Antarctica, *Geophys. Res. Lett.*, *32*, L20311, doi:10.1029/2005GL024296.

Han, S.-C., R. D. Ray, and S. B. Luthcke (2007), Ocean tidal solutions in Antarctica from GRACE inter-satellite tracking data, *Geophys. Res. Lett.*, *34*, L21607, doi:10.1029/2007GL031540.

Han, S., R. Ray, and S. Luthcke (2010), One centimeter-level observations of diurnal ocean tides from global monthly mean time-variable gravity fields, *J. Geod.*, *84*, 715–729.

Jerri, A. (1977), The Shannon sampling theorem—Its various extensions and applications: A tutorial review, *Proc. IEEE*, *65*(11), 1565–1596.

King, M. A., L. Padman, K. Nicholls, P. J. Clarke, G. H. Gudmundsson, B. Kulessa, and A. Shepherd (2011), Ocean tides in the Weddell Sea: New observations on the Filchner-Ronne and Larsen C ice shelves and model validation, *J. Geophys. Res.*, *116*, C06006, doi:10.1029/2011JC006949.

Knudsen, P., and O. Andersen (2002), Correcting GRACE gravity fields for ocean tide effects, *Geophys. Res. Lett.*, *29*(8), 1178, doi:10.1029/2001GL014005.

Luthcke, S., A. Arendt, D. Rowlands, J. McCarthy, and C. Larsen (2008), Recent glacier mass changes in the Gulf of Alaska region from GRACE mascon solutions, *J. Glaciol.*, *54*(188), 767–777.

Lyard, F., F. Lefevre, T. Letellier, and O. Francis (2006), Modelling the global ocean tides: Modern insights from FES2004, *Ocean Dyn.*, *56*(5), 394–415.

McCarthy, D., and G. Petit (2004), IERS conventions (2003), *IERS Tech. Note*, *32*, Int. Earth Rotation and Ref. Syst. Serv., Frankfurt am Main, Germany.

Melachroinos, S., J. Lemoine, P. Tregoning, and R. Biancale (2009), Quantifying FES2004 S 2 tidal model from multiple space-geodesy techniques, GPS and GRACE, over North West Australia, *J. Geod.*, *83*(10), 915–923.

Moore, P., and M. A. King (2008), Antarctic ice mass balance estimates from GRACE: Tidal aliasing effects, *J. Geophys. Res.*, *113*, F02005, doi:10.1029/2007JF000871.

Press, W., S. Teukolsky, W. Vetterling, and B. Flannery (1992), *Numerical Recipes in C*, Cambridge Univ. Press, New York.

Ray, R., and S. Luthcke (2006), Tide model errors and GRACE gravimetry: Towards a more realistic assessment, *Geophys. J. Int.*, *167*(3), 1055–1059.

Ray, R., D. Rowlands, and G. Egbert (2003), Tidal models in a new era of satellite gravimetry, *Space Sci. Rev.*, *108*(1), 271–282.

Ray, R. D., S. B. Luthcke, and J.-P. Boy (2009), Qualitative comparisons of global ocean tide models by analysis of intersatellite ranging data, *J. Geophys. Res.*, *114*, C09017, doi:10.1029/2009JC005362.

Scharroo, R. (2006), Fixing the S1 wave of FES2004, Altimetrics LLC, Cornish, N. H.

Schwiderski, E. (1980), On charting global ocean tides, *Rev. Geophys.*, *18*(1), 243–268.

Steele, M., and W. Ermold (2007), Steric sea level change in the Northern Seas, *J. Clim.*, *20*(3), 403–417.

Swenson, S., D. Chambers, and J. Wahr (2008), Estimating geocenter variations from a combination of GRACE and ocean model output, *J. Geophys. Res.*, *113*, B08410, doi:10.1029/2007JB005338.

Tapley, B. D., S. Bettadpur, M. Watkins, and C. Reigber (2004a), The gravity recovery and climate experiment: Mission overview and early results, *Geophys. Res. Lett.*, *31*, L09607, doi:10.1029/2004GL019920.

Tapley, B., B. Schutz, and G. Born (2004b), *Statistical Orbit Determination*, Academic, Burlington, Mass.

Turing, A. M. (1948), Rounding-off errors in matrix processes, *Q. J. Mech. Appl. Math.*, *1*(1), 287–308.

Wahr, J. (2007), Time variable gravity from satellites, in *Treatise on Geophysics*, vol. 3, *Geodesy*, edited by T. Herring, pp. 213–237, Elsevier, Boston, Mass.

Wang, C., S. Dong, and E. Munoz (2010), Seawater density variations in the North Atlantic and the Atlantic meridional overturning circulation, *Clim. Dyn.*, *34*(7), 953–968.

Willis, J. K., D. P. Chambers, and R. S. Nerem (2008), Assessing the globally averaged sea level budget on seasonal to interannual timescales, *J. Geophys. Res.*, *113*, C06015, doi:10.1029/2007JC004517.

Wu, S., G. Kruizinga, and W. Bertiger (2006), Algorithm Theoretical Basis Document for GRACE level-1B data processing v1.2, *JPL Publ., D-27672*, NASA Jet Propul. Lab., Pasadena, Calif.

S. Desai, M. Watkins, and D. Yuan, Jet Propulsion Laboratory, California Institute of Technology, Pasadena, CA 91109, USA.

E.KillettandJ.Wahr,DepartmentofPhysics,UniversityofColoradoat Boulder, Boulder, CO 80309-0390, USA. (emmykillett@gmail.com)